Efficient imprecise reliability analysis using the Augmented Space Integral

Xiukai Yuan[a,d], Matthias G.R. Faes[b,d,*], Shaolong Liu[a], Marcos A. Valdebenito[c], Michael Beer[d,e,f]

[a]*School of Aerospace and Engineering, Xiamen University, Xiamen 361005, R.P. China*
[b]*KU Leuven, Department of Mechanical Engineering, LMSD Division, Jan De Nayerlaan 5, St.-Katelijne-Waver, Belgium*
[c]*Faculty of Engineering and Sciences, Universidad Adolfo Ibáñez, Av. Padre Hurtado 750, 2562340 Viña del Mar, Chile*
[d]*Institute for Risk and Reliability, Leibniz Universität Hannover, Callinstr. 34, Hannover, Germany*
[e]*Institute for Risk and Uncertainty, University of Liverpool, Peach Street, L69 7ZF Liverpool, United Kingdom*
[f]*International Joint Research Center for Engineering Reliability and Stochastic Mechanics, Tongji University, Shanghai 200092, China*

Abstract

This paper presents an efficient approach to compute the bounds on the reliability of a structure subjected to uncertain parameters described by means of imprecise probabilities. These imprecise probabilities arise from epistemic uncertainty in the definition of the hyper-parameters of a set of random variables that describe aleatory uncertainty in some of the structure's properties. Typically, such calculation involves the solution of a so-called double-loop problem, where a crisp reliability problem is repeatedly solved to determine which realisation of the epistemic uncertainties yields the worst or best case with respect to structural safety. The approach in this paper aims at decoupling this double loop by virtue of the Augmented Space Integral. The core idea of the method is to infer a functional relationship between the epistemically uncertain hyper-parameters and the probability of failure. Then, this functional relationship can be used to determine the best and worst case behaviour with respect to the probability of failure. Three case studies are included to illustrate the effectiveness and efficiency of the developed methods.

Keywords: imprecise reliability analysis, simulation-based method, interval variable, augmented space

1. Introduction

Methods for uncertainty quantification are becoming widespread within the engineering community. However, their practical application becomes challenging whenever the analyst is confronted with insufficient data, as prescribing probability density functions that are commonly used

to represent the uncertainty is far from trivial in this case. In such scenario, the framework of imprecise probabilities has been proven to be a viable alternative approach to traditional probabilistic methods [1]. Following the framework of imprecise probabilities, the epistemic uncertainty that results from such lack of data can be explicitly taken into account by considering credal sets of distribution functions that are consistent with the available information [2], as for instance illustrated in the context of fitting data to accelerated life tests [3], system reliability applications [4], model validation [5, 6] or risk-based design optimization [7].

Practically speaking, however, the calculation of the bounds on probabilistic measures such as the probability of failure based on these credal sets of distributions is hindered by the non-negligible computational cost that is associated with propagating both sources of uncertainty (aleatory and epistemic) jointly towards the model responses, even when simplified imprecise probability models such as parametrized p-boxes are considered [8]. Typically, double loop approaches are deployed to propagate these uncertainties, where the outer loop scans the parameter space spanned by the epistemic uncertainties, while the inner loop calculates a failure probability for each realisation within this epistemic space. There is considerable research effort aimed at reducing this computational cost. For instance, series expansion methods have been introduced (see e.g., [9], [10]) to approximate the epistemic uncertain parameters via series expansion or orthogonal polynomial expansion schemes (see e.g., [11]), or Chebyshev polynomial based schemes such as presented in [12]. For a more rigorous analysis of Monte Carlo methods for propagating imprecise probabilities, the reader is referred to [13, 14]. However, due to assumptions on the local nature of the solution manifold around the expansion point, these methods are often limited to small-to-moderate levels of epistemic uncertainty [15]. An alternative approach lies in the reduction of the computational cost associated with the deterministic solution of the considered model. In this context, many efficient surrogate modelling schemes for the propagation of imprecise probabilistic problems have been proposed using sparse polynomial chaos expansion representations of the model (see e.g., [16, 17]), support vector machines [18], interval predictor models [19, 20] or variants of the Sobol-Hoeffding decomposition (also known as HDMR representation) of the relation between the epistemic parameters and the probability of failure [21, 22], providing an efficient and accurate approximation of the problem. Some of the aforementioned methods even allow performing a global sensitivity analysis of the model, as reported in e.g. [17, 22]. Yet another group of methods are the so-called 'decoupling approaches', which aim at decoupling the earlier described double

loop. For instance, the Operator Norm framework, as presented in recent work by some of the authors (see [23, 24, 25]) is proven to be extremely efficient, but its application is limited to linear models. Finally, the idea of using augmented space methods, as introduced by [26] in the context of probabilistic failure analysis and further developed for sensitivity analysis and reliability-based optimization in, e.g. [27, 28, 29, 30, 31, 32], might also provide a solid foundation to build strategies to reduce the computational cost. In the context of imprecise probabilities, similar methods were introduced by [21, 22, 33] and independently by [34] in a different form. Following these approaches, the main idea is to propagate the epistemic and aleatory uncertainty jointly in a purely aleatory, augmented space that is optimal with respect to a certain well-defined measure, in such a way that both sources of uncertainty can be decoupled again at the response side.

The contribution presented in this paper in fact is a combination of the latter two classes of methods. The core idea is to employ the propagation of the uncertainty in augmented space to derive a functional relationship between the epistemic uncertain parameters and the probability of failure, which is then used to decouple the double loop. This relationship is established by virtue of Bayes' theorem. The work is closely related to recent work of the authors [35], where the Augmented Space Integral method (ASI) is integrated within the Directional Importance Sampling [36] for the efficient calculation of the bounds on the first excursion probability of linear systems subjected to a Gaussian excitation. The contributions in this paper reach wider than the methods described in [35] since they are applicable to nonlinear models, as well as non-Gaussian uncertainties. This is specifically obtained by integrating advanced simulation methods such as Subset Simulation and Importance Sampling into the ASI framework. This contribution is organized as follows. In Section 2, the definition of imprecise reliability analysis problem is first briefly given. Then, the mathematical formulation of the proposed framework is developed in Section 3. Then, in Section 4, various examples are presented to show the performance of the proposed approach. Finally, Section 5 lists the conclusions of the paper.

2. Imprecise reliability

In general, the uncertain parameters of the structure under consideration can be represented using two kinds of variables: imprecise (subjective) random variables and crisp (objective) random variables. The objective random variables represent the aleatory uncertainty on the actual model quantity via a probability density function (PDF) $f(\boldsymbol{y})$. These random variables are for the

remainder of this paper denoted as $\boldsymbol{y} = [y_1, \cdots, y_{n_y}]^T$, with $n_y \in \mathbb{N}$ the number of crisp random variables. The imprecise random variables on the other hand take subjectivity in the definition of the probability density function explicitly into account by considering a set of probabilistic measures. Under this assumption, an imprecise random variable vector $\boldsymbol{x} = [x_1, x_2, \ldots, x_n]^T$ is described by a credal set of probability measures to fully represent all sources of uncertainty. However, the application of the general framework of imprecise probability theory requires complex mathematical descriptions and methods. Therefore, simplified imprecise probability models such as parametric p-boxes are often preferable for a simpler utilization and representation [1]. Given a precise joint probability distribution function (PDF) $f(\boldsymbol{x})$, which is parameterized by a vector $\boldsymbol{\theta} \in \mathbb{R}^n$, a parametric p-box can be represented by the function $f\left(\boldsymbol{x}|\boldsymbol{\theta}\right)$, which depends on a set of interval variables $\boldsymbol{\theta} = [\theta_1, \cdots, \theta_n]^T$, where $\boldsymbol{\theta} \in [\boldsymbol{\theta}_L, \boldsymbol{\theta}_U]$. Given these sources of uncertainty, the analyst is typically concerned with calculating the lower and upper bound of the failure probability, which are given as follows:

$$P_F^L = \min_{\boldsymbol{\theta}\in[\boldsymbol{\theta_L},\boldsymbol{\theta_U}]} P\{G = g(\boldsymbol{x},\boldsymbol{y}) \leq 0\} = \min_{\boldsymbol{\theta}\in[\boldsymbol{\theta_L},\boldsymbol{\theta_U}]} \int I_F(\boldsymbol{x},\boldsymbol{y}) f(\boldsymbol{x}|\boldsymbol{\theta}) f(\boldsymbol{y}) \mathrm{d}\boldsymbol{x} \mathrm{d}\boldsymbol{y} \tag{1}$$

$$P_F^U = \max_{\boldsymbol{\theta}\in[\boldsymbol{\theta_L},\boldsymbol{\theta_U}]} P\{G = g(\boldsymbol{x},\boldsymbol{y}) \leq 0\} = \max_{\boldsymbol{\theta}\in[\boldsymbol{\theta_L},\boldsymbol{\theta_U}]} \int I_F(\boldsymbol{x},\boldsymbol{y}) f(\boldsymbol{x}|\boldsymbol{\theta}) f(\boldsymbol{y}) \mathrm{d}\boldsymbol{x} \mathrm{d}\boldsymbol{y} \tag{2}$$

where $G = g(\boldsymbol{x},\boldsymbol{y})$ is the response function or performance function; $F = \{(\boldsymbol{x},\boldsymbol{y}) : g(\boldsymbol{x},\boldsymbol{y}) \leq 0\}$, is the failure domain; $I_F(\boldsymbol{x},\boldsymbol{y})$ is the indicator function of the failure domain, $I_F(\boldsymbol{x},\boldsymbol{y}) = 1$ if $(\boldsymbol{x},\boldsymbol{y}) \in F$, and $I_F(\boldsymbol{x},\boldsymbol{y}) = 0$ if $(\boldsymbol{x},\boldsymbol{y}) \notin F$. From an engineering point of view, the random variables are assumed to be independent. Note that this assumption does not affect the generality, since dependent random variables can be orthogonalized using appropriate transformations [37]. Concerning the solution of the integral equations in the 'inner' loop of Eq. (1) and Eq. (2), it is well documented that the application of quadrature schemes is unfeasible for most realistic applications [38], even though lower/upper bounds [39] or approximate solutions [30] exist in certain cases. Therefore, the integral equation is usually solved by asymptotic approximations [40] or advanced simulation methods such as Subset Simulation [41], Importance Sampling [42], Directional Importance Sampling [36] or the Probability Density Evolution Method [43] in case of stochastic dynamics. To determine the bounds of P_F using Eqs. (1) and (2), a solution of this integral equation is required at each realisation of $\boldsymbol{\theta}$ that the optimization algorithm in the outer loop generates.

Apart from nearly-trivial cases, such solution is numerically intractable without resorting to either high-performance computing infrastructures or surrogate modelling approaches, since depending on the problem, $\mathcal{O}(2)$ to $\mathcal{O}(6)$ reliability problems need to be solved (see e.g. [23], for numerical examples), each potentially requiring $\mathcal{O}(3) - \mathcal{O}(6)$ deterministic model evaluations depending on the applied simulation method, the order of magnitude of P_F and the desired variance on this estimator. Herein, $\mathcal{O}$ is used to denote 'order of magnitude'.

3. Proposed approach

This section presents an efficient approach to approximate the solution to Eqs. (1) and (2) without having to solve the associated double-loop problem. This method is based on the Augmented Space Integral (ASI) method, as also introduced by some of the authors in [32] in the context of reliability based design optimization. In essence, the proposed approach aims at replacing the integral equation in the 'inner' loop of Eqs. (1) and (2) by an *a priori* defined functional relationship between the failure probability and the epistemic parameters $\boldsymbol{\theta}$, i.e., $P_F(\boldsymbol{\theta})$. Then, based on $P_F(\boldsymbol{\theta})$, the lower and upper bound, respectively P_F^L and P_F^U, are obtained. Section 3.1 describes the basic formulation of the proposed approach. Section 3.2, Section 3.3 and Section 3.4 then illustrate how the formulation can be applied using three simulation-based methods: Monte Carlo simulation, Importance Sampling and Subset Simulation, respectively. Section 3.5 summarizes the procedure of the proposed ASI methodology to provide a practical guide on how to apply this method.

3.1. Augmented space integral

The augmented space idea provides an efficient means for calculating the Failure Probability Function (FPF) $P_F(\boldsymbol{\theta})$ and was first proposed by Au [44]. In an augmented space, the epistemically uncertain hyper-parameter vector $\boldsymbol{\theta}$ is no longer characterized as an interval but it is modeled as a random variable vector with an instrumental probability distribution $\varphi(\boldsymbol{\theta})$. Note that $\varphi(\boldsymbol{\theta})$ is solely used as a numerical tool to estimate the FPF and not as a means to describe the uncertainty on $\boldsymbol{\theta}$, as this would obviously violate the interval paradigm. Then, applying Bayesian theory, $P_F(\boldsymbol{\theta})$ can be calculated as [44]:

$$P_F(\boldsymbol{\theta}) = \frac{\varphi(\boldsymbol{\theta} \mid F) P(F)}{\varphi(\boldsymbol{\theta})} \tag{3}$$

where the instrumental distribution $\varphi(\boldsymbol{\theta})$ can be selected arbitrarily, for example, either Gaussian or Uniform distributions can be employed [44]; $P(F)$ is the failure probability of the augmented

space problem, that is:

$$P(F) = \iint I_F(\boldsymbol{x}, \boldsymbol{y}) f(\boldsymbol{x} \mid \boldsymbol{\theta}) \varphi(\boldsymbol{\theta}) f(\boldsymbol{y}) \mathrm{d}\boldsymbol{\theta} \mathrm{d}\boldsymbol{x} \mathrm{d}\boldsymbol{y} \tag{4}$$

which can be estimated using any suitable reliability method; and $\varphi(\boldsymbol{\theta} \mid F)$ is the posterior distribution of $\boldsymbol{\theta}$ conditioned on the occurrence of the failure event, which can be estimated by performing reliability analysis in the augmented space. The challenge for practical application of Eq. (3) lies usually in the estimation of $\varphi(\boldsymbol{\theta} \mid F)$. In [44], histograms are used to represent $\varphi(\boldsymbol{\theta} \mid F)$ in order to analyze the reliability sensitivity with respect to design parameters for dynamic structural systems. Alternatively, in [27], the Maximum Entropy method is adopted to approximate the posterior distribution, leading to an estimator for $P_F(\boldsymbol{\theta})$ which is an explicit expression of $\boldsymbol{\theta}$. It was further applied to the solution of reliability-based design optimization problems of dynamic systems in [28].

In this contribution, the framework provided by the augmented space concept is further developed, such that there is no need to fit a density function to describe the posterior distribution $\varphi(\boldsymbol{\theta} \mid F)$. For this purpose, recall that the target distribution $\varphi(\boldsymbol{\theta} \mid F)$ is equal to:

$$\varphi(\boldsymbol{\theta} \mid F) = \int \varphi(\boldsymbol{\theta} \mid (\boldsymbol{x}, \boldsymbol{y}), F) f((\boldsymbol{x}, \boldsymbol{y}) \mid F) \mathrm{d}\boldsymbol{x} \mathrm{d}\boldsymbol{y} \tag{5}$$

where the expression of $\varphi(\boldsymbol{\theta} \mid (\boldsymbol{x}, \boldsymbol{y}), F)$ is given by (see Appendix A for the detailed mathematical derivation):

$$\varphi(\boldsymbol{\theta} \mid (\boldsymbol{x}, \boldsymbol{y}), F) = I_F(\boldsymbol{x}, \boldsymbol{y}) \frac{f(\boldsymbol{x} \mid \boldsymbol{\theta})}{\Delta(\boldsymbol{x})} \tag{6}$$

with $\Delta(\boldsymbol{x}) = E_{\boldsymbol{\theta}} \left[(f(\boldsymbol{x} \mid \boldsymbol{\theta}))(\varphi(\boldsymbol{\theta}))^{-1} \right]$, where $E_{\boldsymbol{\theta}}[\cdot]$ represents expectation with respect to $\boldsymbol{\theta}$. The second term in the integral in Eq. (5), that is $f(\boldsymbol{x}, \boldsymbol{y} \mid F)$, can be expressed as shown below.

$$f(\boldsymbol{x}, \boldsymbol{y} \mid F) = \frac{I_F(\boldsymbol{x}, \boldsymbol{y}) f(\boldsymbol{x}, \boldsymbol{y})}{\int I_F(\boldsymbol{x}, \boldsymbol{y}) \int f(\boldsymbol{x}, \boldsymbol{y}, \boldsymbol{\theta}) \mathrm{d}\boldsymbol{\theta} \mathrm{d}\boldsymbol{x} \mathrm{d}\boldsymbol{y}} = \frac{I_F(\boldsymbol{x}, \boldsymbol{y}) f(\boldsymbol{x}, \boldsymbol{y})}{P(F)} \tag{7}$$

Substitution of Eqs. (6) and (7) into Eq. (5) allows rewriting $\varphi(\boldsymbol{\theta} \mid F)$ as:

$$\varphi(\boldsymbol{\theta} \mid F) = \frac{1}{P(F)} \int \frac{I_F(\boldsymbol{x}, \boldsymbol{y}) f(\boldsymbol{x} \mid \boldsymbol{\theta})}{\Delta(\boldsymbol{x})} f(\boldsymbol{x}, \boldsymbol{y}) \mathrm{d}\boldsymbol{x} \mathrm{d}\boldsymbol{y} \tag{8}$$

Finally, substitution of Eq. (8) into Eq. (3) leads to the sought expression for the FPF, that is $P_F(\boldsymbol{\theta})$, which is equal to:

$$P_F(\boldsymbol{\theta}) = \frac{1}{\varphi(\boldsymbol{\theta})} \int \frac{I_F(\boldsymbol{x},\boldsymbol{y}) f(\boldsymbol{x} \mid \boldsymbol{\theta})}{\Delta(\boldsymbol{x})} f(\boldsymbol{x},\boldsymbol{y}) \mathrm{d}\boldsymbol{x}$$
$$= \frac{1}{\varphi(\boldsymbol{\theta})} E\left[\frac{I_F(\boldsymbol{x},\boldsymbol{y}) f(\boldsymbol{x} \mid \boldsymbol{\theta})}{\Delta(\boldsymbol{x})}\right] \tag{9}$$

where $E[\cdot]$ represents expectation under the marginal distribution $f(\boldsymbol{x},\boldsymbol{y})$. This equation reveals that the calculation of FPF $P_F(\boldsymbol{\theta})$ reduces to determining the expected value described in Eq. (9). This expected value can be computed using simulation methods, as will be illustrated in the next sections. This implies that Eq. (9) actually provides a means for determining the functional form of the failure probability as a function of the distribution parameters.

Then, to compute the bounds on P_F, i.e., P_F^L and P_F^U, the following optimization problems have to be solved:

$$P_F^L = \min_{\boldsymbol{\theta} \in [\boldsymbol{\theta_L}, \boldsymbol{\theta_U}]} P_F(\boldsymbol{\theta}) \tag{10}$$

to determine the lower bound, and

$$P_F^U = \max_{\boldsymbol{\theta} \in [\boldsymbol{\theta_L}, \boldsymbol{\theta_U}]} P_F(\boldsymbol{\theta}) \tag{11}$$

to determine the upper bound. As such, rather than solving a reliability problem for each step of the outer loop optimization, the approximation of the bounds is reduced to solving a single reliability problem in augmented space, followed by two deterministic optimization problems over the a priori defined function $P_F(\boldsymbol{\theta})$ as given in Eq. (9). The next sections deal with specific implementation strategies to compute $P_F(\boldsymbol{\theta})$ in an efficient way using simulation methods

3.2. Implementation with Monte Carlo simulation

The most straightforward implementation to solve the integral in Eq. (9) is to apply Monte Carlo simulation. Note that Monte Carlo simulation is applied in the augmented space $(\boldsymbol{x},\boldsymbol{y},\boldsymbol{\theta})$. As such, samples of $f(\boldsymbol{x},\boldsymbol{y}) = f(\boldsymbol{x})f(\boldsymbol{y})$ are generated, and the estimate can be readily obtained. The procedure is denoted in the following as 'ASI-MCS' and is described below.

1. Generate samples of $f(\boldsymbol{x})$. As $f(\boldsymbol{x})$ is a marginal distribution, it cannot be directly sampled since there may be no closed-form expression in the general case. Therefore, sampling from this distribution has to be performed as follows. First, generate samples $\left\{\boldsymbol{\theta}^{(j)}, j = 1,\ldots,N\right\}$ that follow $\varphi(\boldsymbol{\theta})$. Then, for each of these samples, generate samples $\left\{\boldsymbol{x}^{(j)}, j = 1,\ldots,N\right\}$, each of them distributed according to $f\left(\boldsymbol{x} \mid \boldsymbol{\theta}^{(j)}\right)$. As such, a set of samples $\left\{\left(\boldsymbol{x}^{(j)}, \boldsymbol{\theta}^{(j)}\right), j = 1,\ldots,N\right\}$

that follows $f(\boldsymbol{x}, \boldsymbol{\theta})$ is obtained. Based on these samples, and discarding the samples $\boldsymbol{\theta}^{(j)}$, the remaining set of samples $\left\{\boldsymbol{x}^{(j)}, j = 1, \ldots, N\right\}$ is distributed as the marginal distribution $f(\boldsymbol{x})$.

2. Generate samples from $f(\boldsymbol{y})$. In this sense, note that a number of samples can be directly generated from $f(\boldsymbol{y})$.

3. Compute the estimate for $P_F(\boldsymbol{\theta})$ based on the samples set $\left\{\left(\boldsymbol{x}^{(j)}, \boldsymbol{y}^{(j)}\right), j = 1, \ldots, N\right\}$ as:

$$\hat{P}_F(\boldsymbol{\theta}) = \frac{1}{\varphi(\boldsymbol{\theta})} \frac{1}{N} \sum_{j=1}^{N} \frac{I_F\left(\boldsymbol{x}^{(j)}, \boldsymbol{y}^{(j)}\right) f\left(\boldsymbol{x}^{(j)} \mid \boldsymbol{\theta}\right)}{\Delta\left(\boldsymbol{x}^{(j)}\right)} \tag{12}$$

The estimator $\hat{P}_F(\boldsymbol{\theta})$ is obviously unbiased, and its variance is:

$$\mathrm{Var}\left[\hat{P}_F(\boldsymbol{\theta})\right] \approx \frac{1}{N-1} \left\{ \frac{1}{N} \sum_{j=1}^{N} \left\{ \frac{I_F\left(\boldsymbol{x}^{(j)}, \boldsymbol{y}^{(j)}\right) f\left(\boldsymbol{x}^{(j)} \mid \boldsymbol{\theta}\right)}{\varphi(\boldsymbol{\theta}) \Delta\left(\boldsymbol{x}^{(j)}\right)} \right\}^2 - \hat{P}_F^2(\boldsymbol{\theta}) \right\} \tag{13}$$

It should be noted that the proposed ASI approach is implemented by using MCS only once to obtain the failure probability as a function. In other words, a single run of MCS suffices for determining the failure probability as an explicit function of $\boldsymbol{\theta}$. Hence, repeated reliability analyses are avoided and the double loop is effectively broken, as illustrated in Eqs. (10) and (11). It is expected that carrying out ASI-MCS should be more efficient from a numerical viewpoint than applying MCS for specific crisp values of $\boldsymbol{\theta}$. This is due to the fact that a relatively large failure probability is estimated in the augmented space ($P(F)$ in Eq. (4)), in opposition to a possibly small failure probability $P_F(\boldsymbol{\theta})$ for certain values of $\boldsymbol{\theta}$.

3.3. Implementation with Importance Sampling

The proposed framework as cast in Eqs. (9), (10) and (11) can also be implemented using Importance Sampling, which is denoted as 'ASI-IS' for the remainder of the paper. Introducing an appropriate Importance Sampling function $H(\boldsymbol{x}, \boldsymbol{y})$ in the augmented space, the formulation for $P_F(\boldsymbol{\theta})$ in Eq. (9) can be rewritten as:

$$P_F(\boldsymbol{\theta}) = \frac{1}{\varphi(\boldsymbol{\theta})} \int \frac{I_F(\boldsymbol{x}, \boldsymbol{y}) f(\boldsymbol{x} \mid \boldsymbol{\theta})}{\Delta(\boldsymbol{x})} \frac{f(\boldsymbol{x}, \boldsymbol{y})}{H(\boldsymbol{x}, \boldsymbol{y})} H(\boldsymbol{x}, \boldsymbol{y}) \mathrm{d}\boldsymbol{x} \mathrm{d}\boldsymbol{y} \tag{14}$$

In an augmented space, it may not be straightforward to select an optimal Importance Sampling function. Here, the following approach is adopted for determining $H(\boldsymbol{x}, \boldsymbol{y})$. The design point associated with the performance function can be solved with respect to a nominal value of the epistemic uncertain parameter, for example, $\boldsymbol{\theta}_0$. This nominal value can be simply set as the

center of the hyper-rectangular domain associated with $\boldsymbol{\theta}$, i.e., $\boldsymbol{\theta}_0 = (\boldsymbol{\theta}_L + \boldsymbol{\theta}_U)/2$. Then, based on the design point, which is denoted as $[\boldsymbol{x}^*, \boldsymbol{y}^*]$, $H(\boldsymbol{x}, \boldsymbol{y})$ can be chosen as:

$$H(\boldsymbol{x}, \boldsymbol{y}) = f(\boldsymbol{x}) H(\boldsymbol{y}|\boldsymbol{y}^*) \tag{15}$$

where $f(\boldsymbol{x})$ is the marginal distribution associated with $\boldsymbol{x}$ and $H(\boldsymbol{y}|\boldsymbol{y}^*)$ denotes the Importance Sampling density function associated with $\boldsymbol{y}$. The density $H(\boldsymbol{y}|\boldsymbol{y}^*)$ is equal to $f(\boldsymbol{y})$ except for its expected value, which is set equal to $\boldsymbol{y}^*$. Please note that $\boldsymbol{x}^*$ is not included in the Importance Sampling density $H(\boldsymbol{x}, \boldsymbol{y})$ to allow exploring the failure region associated with different values of $\boldsymbol{\theta}$. An alternative approach for selecting $H(\boldsymbol{x}, \boldsymbol{y})$ could be based on an adaptive Importance Sampling density [45].

Substituting Eq. (15) into (14) and considering that $f(\boldsymbol{x}, \boldsymbol{y}) = f(\boldsymbol{x}) f(\boldsymbol{y})$ and $f(\boldsymbol{x}) = \varphi(\boldsymbol{\theta}) \Delta(\boldsymbol{x})$ allows rewriting $P_F(\boldsymbol{\theta})$ as:

$$\begin{aligned} P_F(\boldsymbol{\theta}) &= \frac{1}{\varphi(\boldsymbol{\theta})} \int \frac{I_F(\boldsymbol{x}, \boldsymbol{y}) f(\boldsymbol{x} \mid \boldsymbol{\theta})}{\Delta(\boldsymbol{x})} \frac{f(\boldsymbol{x}, \boldsymbol{y})}{f(\boldsymbol{x}) H(\boldsymbol{y}|\boldsymbol{y}^*)} f(\boldsymbol{x}) H(\boldsymbol{y}|\boldsymbol{y}^*) \mathrm{d}\boldsymbol{x} \mathrm{d}\boldsymbol{y} \\ &= \frac{1}{\varphi(\boldsymbol{\theta})} E_H \left[\frac{I_F(\boldsymbol{x}, \boldsymbol{y}) f(\boldsymbol{x} \mid \boldsymbol{\theta}) f(\boldsymbol{y})}{\Delta(\boldsymbol{x}) H(\boldsymbol{y}|\boldsymbol{y}^*)} \right] \end{aligned} \tag{16}$$

where $E_H[\cdot]$ denotes the expectation under $H(\boldsymbol{x}, \boldsymbol{y})$ in the augmented space.

In case a suitable Importance Sampling density function has been chosen, then samples can be generated according to $H(\boldsymbol{x}, \boldsymbol{y})$. Suppose that a total of N samples are generated, that is $\left\{ (\boldsymbol{x}^{(j)}, \boldsymbol{y}^{(j)}), j = 1, \ldots, N \right\}$. Then, according to Eq. (16), $P_F(\boldsymbol{\theta})$ is estimated as:

$$\hat{P}_F(\boldsymbol{\theta}) = \frac{1}{\varphi(\boldsymbol{\theta})} \frac{1}{N} \sum_{j=1}^{N} \frac{I_F\left(\boldsymbol{x}^{(j)}, \boldsymbol{y}^{(j)}\right) f\left(\boldsymbol{x}^{(j)} \mid \boldsymbol{\theta}\right)}{\Delta(\boldsymbol{x})^{(j)}} \frac{f\left(\boldsymbol{y}^{(j)}\right)}{H\left(\boldsymbol{y}^{(j)}|\boldsymbol{y}^*\right)} \tag{17}$$

This estimator $\hat{P}_F(\boldsymbol{\theta})$ is also unbiased, and its variance is:

$$\mathrm{Var}\left[\hat{P}_F(\boldsymbol{\theta})\right] \approx \frac{1}{N-1} \left\{ \frac{1}{N} \sum_{j=1}^{N} \left\{ \frac{I_F\left(\boldsymbol{x}^{(j)}, \boldsymbol{y}^{(j)}\right) f\left(\boldsymbol{x}^{(j)} \mid \boldsymbol{\theta}\right)}{\varphi(\boldsymbol{\theta}) \Delta\left(\boldsymbol{x}^{(j)}\right)} \frac{f\left(\boldsymbol{y}^{(j)}\right)}{H\left(\boldsymbol{y}^{(j)}|\boldsymbol{y}^*\right)} \right\}^2 - \hat{P}_F^2(\boldsymbol{\theta}) \right\} \tag{18}$$

3.4. Implementation with Subset Simulation

Subset Simulation is an efficient reliability analysis method which is capable of dealing with high dimensional problems, nonlinear performance functions and failure events of rare occurrence [46]. It expresses a low failure probability as the product of a series of conditional but larger probabilities, and utilizes Markov Chain Monte Carlo (MCMC) simulation to efficiently calculate these

probabilities. The proposed ASI framework can be implemented together with Subset Simulation, as described in the following.

Suppose that in the augmented space $(\boldsymbol{x}, \boldsymbol{y}, \boldsymbol{\theta})$, a nested sequence of failure events is defined such that $F_1 \supset F_2 \supset \ldots \supset F_m = F$, where $F_i = \{g(\boldsymbol{x}, \boldsymbol{y}) \leq b_i\} (i = 1, 2, \ldots, m)$ and $b_i,\ i = 1, \ldots, m$ denote a set of intermediate threshold levels. Then, the failure probability can be expressed as:

$$P(F) = P(F_1) \sum_{i=2}^{m} P(F_i \mid F_{i-1}) \tag{19}$$

The corresponding intermediate threshold values $b_1, b_2, \ldots, b_{m-1}$ are adaptively determined, such that the corresponding probabilities $P(F_1)\ , P(F_2 \mid F_1), \cdots, P(F_{m-1} \mid F_{m-2})$ are set to be equal to p_0, e.g., $p_0 = 0.1$ for convenience. The final threshold $b_m = 0$ is not chosen adaptively.

The practical implementation of Subset Simulation in the augmented space (which is denoted as ASI-SS in the following) is almost identical to the original implementation of Subset Simulation [41]. Specifically, suppose that there are N_s samples generated at the $(\mathrm{m} - 1)^{th}$ stage of Subset Simulation in the augmented space. Moreover, it is considered that there are N_F failure samples located at the final stage such that $\left\{\left(\boldsymbol{x}^{(j)}, \boldsymbol{y}^{(j)}, \boldsymbol{\theta}^{(j)}\right), j = 1, \ldots, N_F\right\}$, which are distributed as $f(\boldsymbol{x}, \boldsymbol{y}, \boldsymbol{\theta} \mid F)$. Discarding the samples corresponding to $\boldsymbol{\theta}$, the samples $\left\{(\boldsymbol{x}^{(j)}, \boldsymbol{y}^{(j)}), j = 1, \ldots, N_F\right\}$ are distributed according to $f((\boldsymbol{x}, \boldsymbol{y}) \mid F)$. Furthermore, recall that the conditional distribution $\varphi(\boldsymbol{\theta} \mid F)$ can be expressed as:

$$\begin{aligned} \varphi(\boldsymbol{\theta} \mid F) &= \int \frac{I_F(\boldsymbol{x}, \boldsymbol{y}) f(\boldsymbol{x} \mid \boldsymbol{\theta})}{\Delta(\boldsymbol{x})} \frac{f(\boldsymbol{x}, \boldsymbol{y})}{P(F)} \mathrm{d}\boldsymbol{x}\mathrm{d}\boldsymbol{y} \\ &= \int \frac{f(\boldsymbol{x} \mid \boldsymbol{\theta})}{\Delta(\boldsymbol{x})} f((\boldsymbol{x}, \boldsymbol{y}) | F) \mathrm{d}\boldsymbol{x}\mathrm{d}\boldsymbol{y} \end{aligned} \tag{20}$$

which can be estimated considering the samples distributed according to $f((\boldsymbol{x}, \boldsymbol{y}) \mid F)$, that is:

$$\hat{\varphi}(\boldsymbol{\theta} \mid F) = \frac{1}{N_F} \sum_{j=1}^{N_F} \frac{f\left(\boldsymbol{x}^{(j)} \mid \boldsymbol{\theta}\right)}{\Delta\left(\boldsymbol{x}^{(j)}\right)} \tag{21}$$

Additionally, the augmented failure probability as defined in Eq. (4) is estimated by means of Subset Simulation according to:

$$\hat{P}(F) = p_0^{m-1} \frac{N_F}{N_s} \tag{22}$$

Finally, substitution of Eqs. (21) and (22) into Eq. (3) leads to the following estimator for the

FPF $P_F(\boldsymbol{\theta})$:

$$\hat{P}_F(\boldsymbol{\theta}) = \frac{p_0^{m-1}}{\varphi(\boldsymbol{\theta})} \frac{1}{N_s} \sum_{j=1}^{N_s} \frac{I_F\left(\boldsymbol{x}^{(j)}, \boldsymbol{y}^{(j)}\right) f\left(\boldsymbol{x}^{(j)} \mid \boldsymbol{\theta}\right)}{\Delta\left(\boldsymbol{x}^{(j)}\right)}. \tag{23}$$

The coefficient of variation (C.O.V.) of the estimator is equal to:

$$\mathrm{Cov}\left[\hat{P}_F(\boldsymbol{\theta})\right] = \sqrt{\sum_{i=1}^{m} \frac{\mathrm{Var}\left(\hat{P}_i\right)}{P_i^2}} \approx \sqrt{\sum_{i=1}^{m} \frac{\mathrm{Var}\left(\hat{P}_i\right)}{\hat{P}_i^2}} \tag{24}$$

Please refer to Appendix B for the details on the derivation of this estimator.

3.5. Summary of the proposed framework

The practical application of the proposed strategy to compute the bounds of P_F in an efficient way can be summarized as follows:

1. Select a distribution $\varphi(\boldsymbol{\theta})$. A feasible choice is a uniform distribution, due to its simplicity.
2. Perform simulation. ASI-MCS, ASI-IS or ASI-SS can be selected to carry out reliability analysis in the augmented space $(\boldsymbol{x}, \boldsymbol{y}, \boldsymbol{\theta})$, producing failure samples $\left\{\left(\boldsymbol{x}^{(j)}, \boldsymbol{y}^{(j)}, \boldsymbol{\theta}^{(j)}\right) : j = 1, \ldots, N_F\right\}$.
3. Obtain the FPF estimator. The FPF can be obtained according to Eq. (12) for ASI-MCS, Eq. (17) for ASI-IS or Eq. (23) for ASI-SS.
4. Imprecise reliability analysis. Solve the optimization problems in Eqs. (10) and (11) to determine the bounds of the failure probability, that is, P_F^L and P_F^U, respectively.

4. Examples

In this section, three examples are presented to illustrate the performance of the proposed strategy. For comparison purposes, the double loop method is also applied. It is implemented by using the class of convex optimization algorithms included in the Matlab function 'fmincon' to solve the 'outer' propagation problem, as shown in Eqs. (1) and (2). The 'inner' loop is solved using a Monte Carlo estimator, where the sample size depends on the actual case study. Furthermore, 'fmincon' is also used to optimize over the failure probability function once the propagation of the imprecise probabilities is decoupled following the proposed strategy (i.e., to solve Eqs. (10) and (11)).

4.1. Example 1

The first example considers the front axle of a car, which is an important component for the structural reliability since it bears heavy loads during operational use [47]. Often, an I-beam profile is used in the design due to its high bending strength and stiffness combined with its comparatively light weight (as compared to e.g., a rectangular cross-section). Fig. 1 shows a diagram of the cross-section of a typical front axle, where the thicknesses of web and flange are denoted as a and t, respectively.

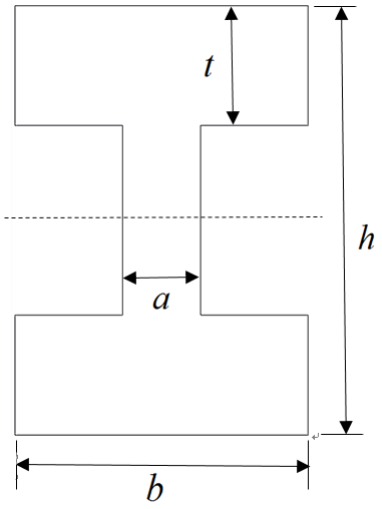

Figure 1: Diagram of automobile front axle.

To verify the static strength behavior of the front axle, the following performance function is formulated:

$$g(\boldsymbol{x}, \boldsymbol{y}) = \sigma_s - \sqrt{\sigma^2 + 3\tau^2} \tag{25}$$

where $\boldsymbol{x} = [a, t]^T$ is the vector of imprecise variables; $\boldsymbol{y} = [b, h, M, T]^T$ is the vector of objective random variables; and σ_s is the yield stress. According to the material property of the front axle, σ_s =680 MPa. The maximum normal stress and shear stress are $\sigma = M/W_x$ and $\tau = T/W_\rho$, where M and T are bending moment and torque, respectively, W_x and W_ρ are the section factor and polar section factor, respectively, which are equal to:

$$W_x = \frac{a(h-2t)^3}{6h} + \frac{b}{6h}\left[h^3 - (h-2t)^3\right] \tag{26}$$

$$W_\rho = 0.8bt^2 + 0.4\left[a^3(h-2t)/t\right] \tag{27}$$

All the variables are assumed to be independent with respect to each other and the probability distributions associated with each of them are listed in Table 1. The mean values of a and t, are

modeled as interval variables, i.e., $\theta_1 = \mu_a \in [11, 13]$ and $\theta_2 = \mu_t \in [13, 15]$, respectively. Note that the distributions of those parameters that must be positive due to physical reasons, i.e., a, t, b and h, are truncated such that no samples with negative values are generated.

Table 1: The distribution information of the random variables in Example 1

Random variable	a(mm)	t(mm)	b(mm)	h(mm)	M(KN $\cdot$ m)	T(KN $\cdot$ m)
Mean value	$\theta_1 \in [11, 13]$	$\theta_2 \in [13, 15]$	65	85	3.5	3.1
Standard deviation	1.2	1.4	6.5	8.5	0.35	0.31
Distribution	Normal	Normal	Normal	Normal	Log-Normal	Log-Normal

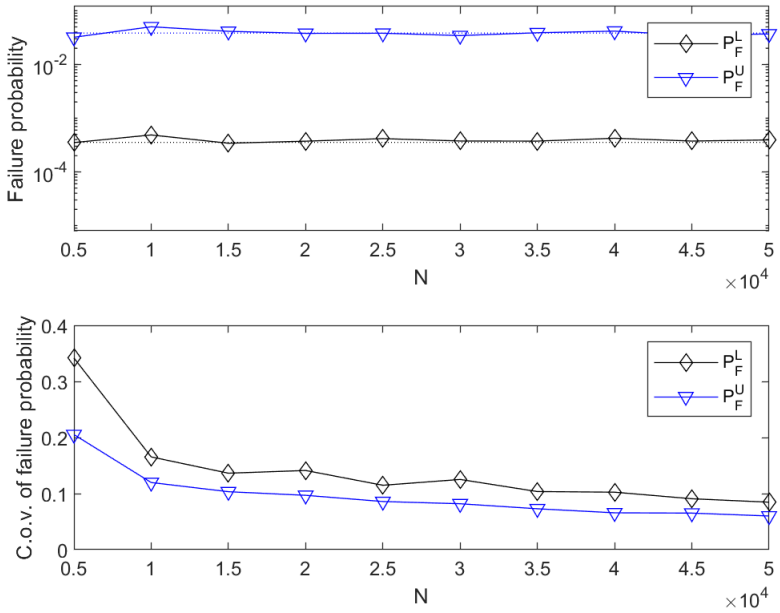

Figure 2: Evolution of the failure probability and its coefficient of variation with respect to the number of samples obtained by ASI-MCS (Example 1).

The proposed approaches, i.e., ASI-MCS ASI-IS and ASI-SS, are applied to carry out the imprecise reliability analysis in the augmented space. First, different sample sizes are used to investigate the performance with respect to the computation cost. Figs. 2, 3 and 4 show the evolution of the results of the proposed ASI-MCS, ASI-IS and ASI-SS, respectively, with respect to the sample set size. Based on this, the bounds for the failure probability ($\hat{P}_F^U$ and $\hat{P}_F^L$) are obtained. It is observed that the three approaches are capable of determining the bounds of the failure probability. Moreover, both ASI-IS and ASI-SS outpeform ASI-MCS, as they require less

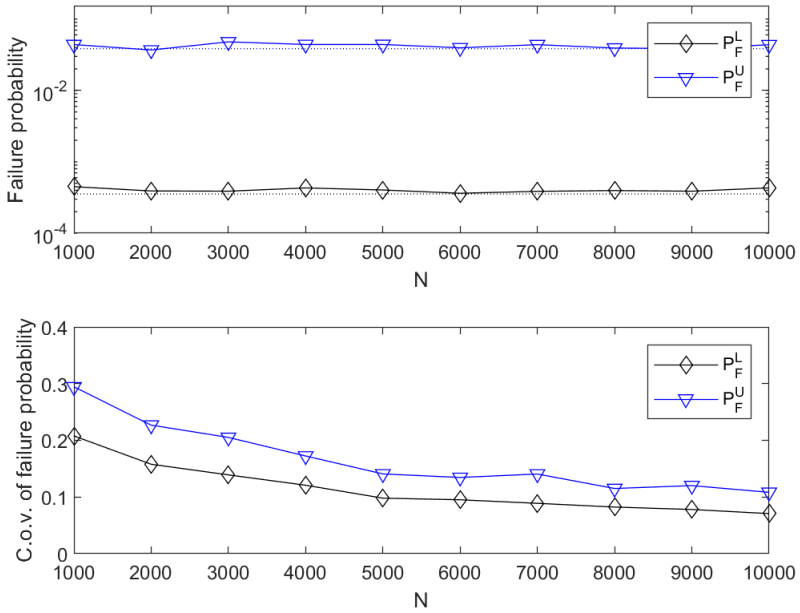

Figure 3: Evolution of the failure probability and its coefficient of variation with respect to the number of samples obtained with ASI-IS (Example 1).

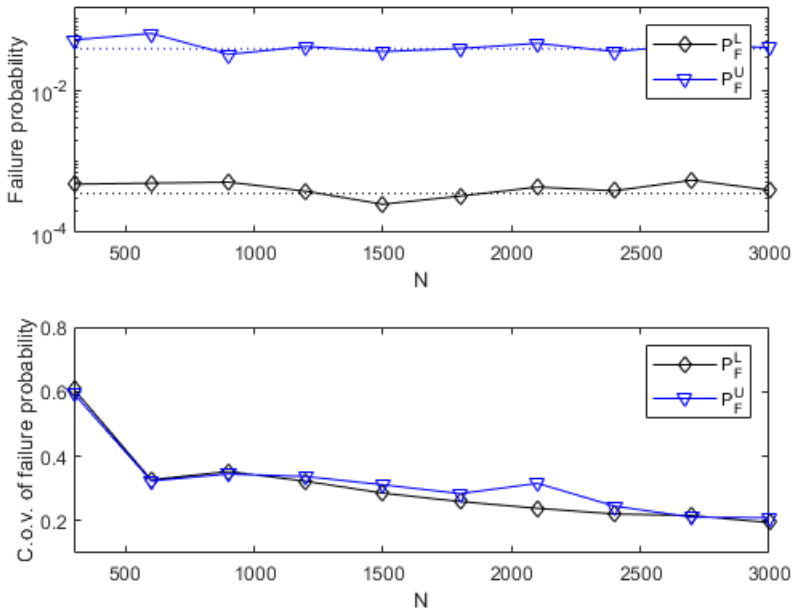

Figure 4: Evolution of the failure probability and its coefficient of variation with respect to the number of samples obtained with ASI-SS (Example 1).

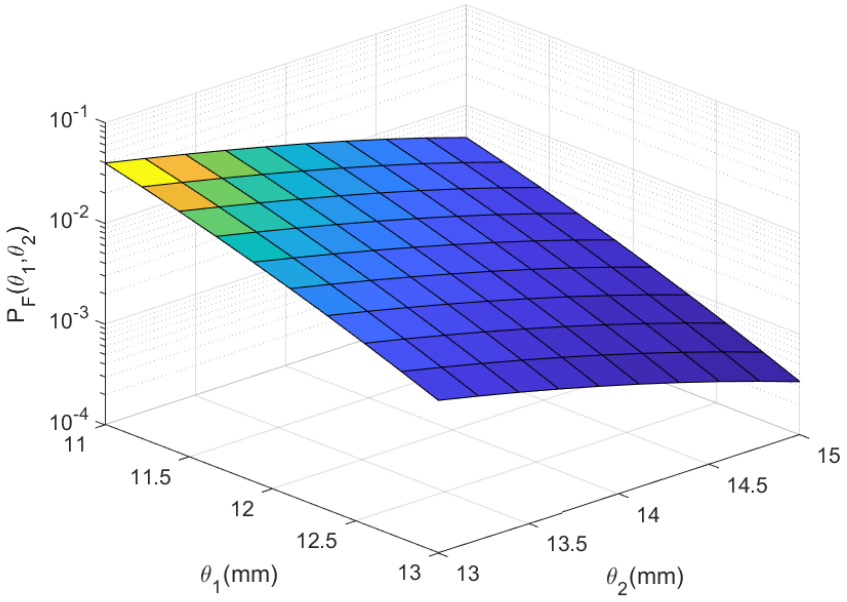

Figure 5: FPF $P_F(\theta_1, \theta_2)$ obtained by ASI-MCS.

samples for producing comparable bounds. This was an expected result, as both Importance Sampling and Subset Simulation are usually more efficient than Monte Carlo.

Based on these results, and considering the balance between the computational cost and accuracy, the following setting of the approaches is used for further analysis: $N = 10^4$ samples for ASI-MCS, $N = 4000$ for ASI-IS (excluding the cost of determining design point) and $N = 6000$ for ASI-SS (where $N_i = 2000,\ i = 1, 2, 3$, samples are considered for each level). As mentioned before, only one reliability analysis in the augmented space is required to estimate the FPF. In order to visualize the results produced by the proposed strategy, the FPF resulting from ASI-MCS is shown in Fig. 5. Furthermore, the FPF obtained by the three proposed approaches are compared in one-dimensional plots, i.e., $P_f\left(\theta_1, \theta_2 = 14\right)$ and $P_f\left(\theta_1 = 12, \theta_2\right)$, as shown in Figs. 6$a$ and 6b, respectively. It can be seen that the results are quite consistent with the exact, point-wise values of FPF obtained by direct MCS with 10^6 samples associated with each point in the curve.

Finally, Table 2 shows the results obtained by performing the calculation of the bounds via the three proposed approaches, as well as a validation using a conventional double-loop Monte Carlo estimation. Specifically, the table shows the obtained estimators for the lower and upper bounds, as well as the coefficient of variation of these estimators. It can be seen from the table that the results obtained by different approaches agree with each other, and that the coefficients of variation associated with the obtained bounds are reasonable taking into account the gain in

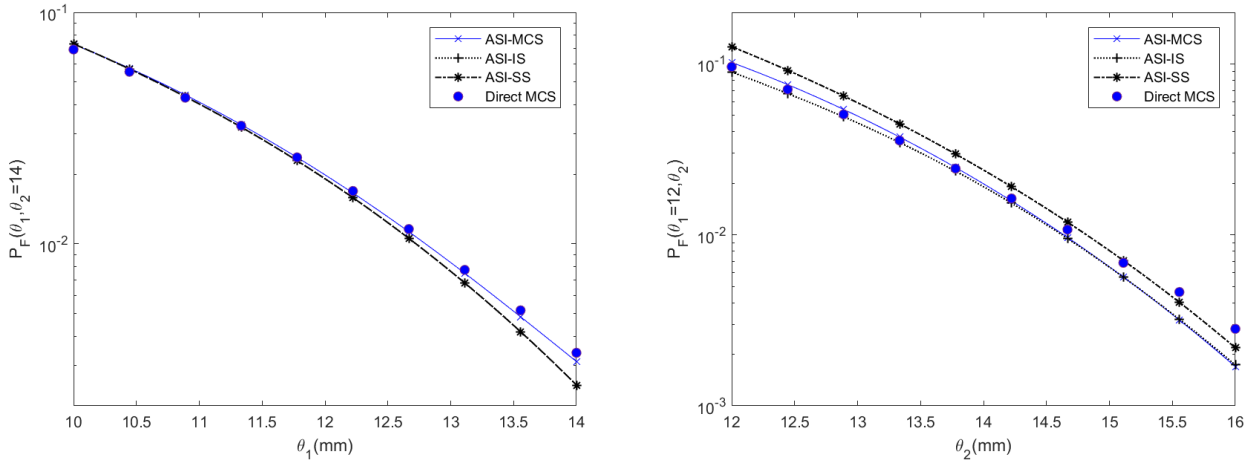

(a) $P_F(\theta_1, \theta_2 = 14)$ (b) $P_F(\theta_1 = 12, \theta_2)$

Figure 6: FPF obtained with the proposed strategy considering Monte Carlo (ASI-MCS), Importance Sampling (ASI-IS) and Subset Simulation (ASI-SS) and comparison with FPF obtained with direct Monte Carlo.

computational efficiency. Of course, the results obtained by the double-loop approach are the most accurate, but they come at a much higher computational cost.

Table 2: Estimated probability bounds and their coefficient of variation for Example 1

Method	$\hat{P}_F^U$	$Cov(\hat{P}_F^U)$	$\hat{P}_F^L$	$Cov(\hat{P}_F^L)$	N
ASI-MCS	0.0368	0.12	3.5176×10^{-4}	0.16	10^4
ASI-IS	0.0305	0.15	3.6401×10^{-4}	0.11	4000
ASI-SS	0.0330	0.24	3.4383×10^{-4}	0.25	3×2000*
Double-loop	0.0384	0.016	3.5400×10^{-4}	0.050	$21 \times 10^5 + 42 \times 10^6$

*3×2000 denotes that Subset Simulation required 3 simulation stages, each of them comprising 2000 samples.

4.2. Example 2: Composite beam

The second case study comprises the analysis of a composite beam model. This example is shown in Fig. 7 and is partially based on the example presented in [48]. The beam has a width of A(mm), a height of B(mm) and a length of L(mm). The Young's modulus of the material is denoted as E_w. In addition, the beam is reinforced by an aluminum plate clamped on the bottom of the beam and whose Young's modulus is denoted as E_a. This aluminum plate possesses a cross section of width C(mm) and height D(mm). The beam is loaded with six external vertical forces, P_1, P_2, P_3, P_4, P_5 and P_6(kN). These forces are applied discrete locations L_1, L_2, L_3, L_4, L_5 and L_6 along its longitudinal direction. Failure is defined as maximum bending normal stress of the beam

exceeding the allowable tensile stress S (strength). The performance function associated with this failure criterion is:

$$g(\boldsymbol{x}, \boldsymbol{y}) = S - \sigma_{\max}(\boldsymbol{x}, \boldsymbol{y}) \tag{28}$$

where $S = 0.0198$ GPa is the allowable tensile stress; $\boldsymbol{x} = [A, B, C, D]^T$ is the vector of imprecise variables; $\boldsymbol{y}$ is the vector of the remaining 15 objective random variables, which are the beam's length, the Young's moduli of the beam and plate, and the locations and magnitudes of the vertical forces; $\sigma_{\max}(\boldsymbol{x}, \boldsymbol{y})$ is the maximum stress given by $\sigma_{\max}(\boldsymbol{x}, \boldsymbol{y}) = \max\{\sigma_k(\boldsymbol{x}, \boldsymbol{y}) : k = 1, \ldots, 6\}$ and $\sigma_k(\boldsymbol{x}, \boldsymbol{y})$ is the stress of the cross-section which given by:

$$\sigma_1(\boldsymbol{x}, \boldsymbol{y}) = \frac{\left[(L_1/L)\sum_{i=1}^{6} P_i\,(L - L_i)\right] Y_{\max}(\boldsymbol{x}, \boldsymbol{y})}{W(\boldsymbol{x}, \boldsymbol{y})} \tag{29}$$

$$\sigma_k(\boldsymbol{x}, \boldsymbol{y}) = \frac{\left[(L_k/L)\sum_{i=1}^{6} P_i\,(L - L_i) - \sum_{i=1}^{k-1} P_i\,(L_k - L_i)\right] Y_{\max}(\boldsymbol{x}, \boldsymbol{y})}{W(\boldsymbol{x}, \boldsymbol{y})} (k = 2, \ldots, 6) \tag{30}$$

where

$$Y_{\max}(\boldsymbol{x}, \boldsymbol{y}) = \frac{0.5AB^2 + DC(B + D)E_a/E_w}{AB + DCE_a/E_w} \tag{31}$$

$$W(\boldsymbol{x}, \boldsymbol{y}) = \frac{AB^3}{12} + AB\left[Y_{\max}(\boldsymbol{x}, \boldsymbol{y}) - \frac{B}{2}\right]^2 + \frac{CD^3E_a}{12E_w} + \frac{CDE_a}{E_w}\left[\frac{D}{2} + B - Y_{\max}(\boldsymbol{x}, \boldsymbol{y})\right]^2 \tag{32}$$

The mean values of A, B, C and D are modeled as interval variables. The distribution information of the random variables is given in Table 3. Note that the distributions of those parameters that must be positive for physical reasons, for example, the geometrical and material properties, are truncated such that no negative samples are generated. Moreover, all random variables are assumed to be independent.

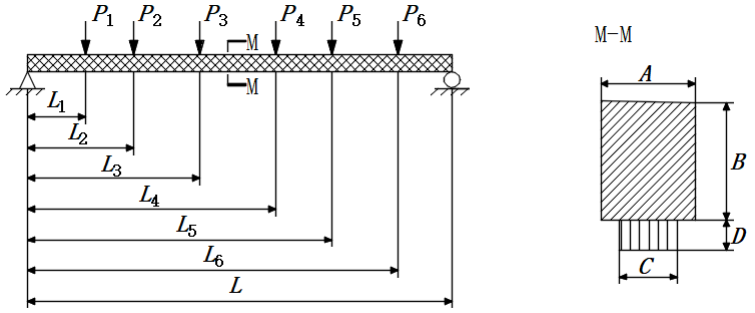

Figure 7: Schematic illustration of the Composite Beam

Table 3: Distribution information of random variables for the composite beam

No.	Random variable	Location parameter	Scale parameter	Distribution
1	A(mm)	$\theta_1 \in [95, 105]$	5	Normal
2	B(mm)	$\theta_2 \in [190, 210]$	10	Normal
3	C(mm)	$\theta_3 \in [75, 85]$	4	Normal
4	D(mm)	$\theta_4 \in [18, 22]$	1	Normal
5	L_1(mm)	200	2	Normal
6	L_2(mm)	400	4	Normal
7	L_3(mm)	600	6	Normal
8	L_4(mm)	800	8	Normal
9	L_5(mm)	1000	10	Normal
10	L_6(mm)	1200	12	Normal
11	L(mm)	1400	14	Normal
12	P_1(KN)	15	3	Extreme value
13	P_2(KN)	15	3	Extreme value
14	P_3(KN)	15	3	Extreme value
15	P_4(KN)	15	3	Extreme value
16	P_5(KN)	15	3	Extreme value
17	P_6(KN)	15	3	Extreme value
18	E_a(GPa)	70	0.7	Normal
19	E_w(GPa)	8.75	0.0875	Normal

The results obtained by the proposed strategy implemented considering Monte Carlo simulation, Importance Sampling and Subset Simulation, as well as the results stemming form a double loop Monte Carlo validation run are shown in Table 4. As noted from the Table, the obtained results agree rather well with the double loop result. It is observed that there exists a slight discrepancy in the calculation of the bounds, which is caused by the fact that the epistemic uncertainty is resolved over an approximation of the FPF. While this introduces small differences, there is a significant gain in computational efficiency. Furthermore, the coefficient of variation (Cov), as also illustrated in Table 4, gives a measure for the statistical accuracy of the estimator.

Table 4: Estimated probability bounds and their coefficient of variation for Example 2

Method	$\hat{P}_F^U$	$Cov(\hat{P}_F^U)$	$\hat{P}_F^L$	$Cov(\hat{P}_F^L)$	N
ASI-MCS	0.4907	0.11	2.0512×10^{-3}	0.12	10^4
ASI-IS	0.4806	0.14	1.8759×10^{-3}	0.16	4000
ASI-SS	0.5040	0.18	2.4228×10^{-3}	0.17	2×2000*
Double-loop	0.4682	0.011	2.25×10^{-3}	0.059	$10\times10^4+93\times10^5$

*2×2000 denotes that Subset Simulation required 2 simulation stages, each of them comprising 2000 samples.

4.3. Example 3: Car road dynamics

4.3.1. General model introduction

The third case study represents a quarter-car model, which is a 2 degree of freedom idealisation of the realistic dynamics of the suspension of a car. Specifically, this case study is concerned with assessing the bounds on several comfort metrics of a vehicle suspension, given several imprecisely defined properties of the system. The quarter-car dynamics can be represented as a set of two ordinary differential equations:

$$m_s\ddot{x}_s + c_s(\dot{x}_s - \dot{x}_{us}) + k_s(x_s - x_{us}) = 0 \tag{33}$$

$$m_{us}\ddot{x}_{us} - c_s(\dot{x}_s - \dot{x}_{us}) - k_s(x_s - x_{us}) + c_t(\dot{x}_{us} - \dot{x}_0) + k_t(x_{us} - x_0) = 0 \tag{34}$$

with $\dot{\bullet}$ the time derivative of $\bullet$, x_{us} the displacement of the unsprung mass (i.e., the suspension components, wheel and other components directly connected to them), x_s the displacement of the sprung mass (i.e., all components resting on the suspension), m_{us} and m_s the unsprung and sprung mass of a quarter of the car, c_s and c_t respectively the damping coefficients of the suspension and tire, k_s and k_t respectively the stiffness coefficients of the suspension and tire. Finally, x_0 and $\dot{x}_0$ are the displacement and velocity in vertical direction that excite the bottom of the wheel (i.e., the road profile). The complete road profile is denoted $x_0(t)$. A schematic representation of the model is given in figure 8.

For the solution of this coupled system of ODEs, a state-space model is employed:

$$\frac{d}{dt}\begin{bmatrix} x_{us}-x_0 \\ \dot{x}_{us} \\ x_s - x_{us} \\ \dot{x}_s \end{bmatrix} = A\begin{bmatrix} x_{us}-x_0 \\ \dot{x}_{us} \\ x_s - x_{us} \\ \dot{x}_s \end{bmatrix} + \begin{bmatrix} -1 \\ \frac{4c_t}{m_{us}} \\ 0 \\ 0 \end{bmatrix}\dot{x}_0 \tag{35}$$

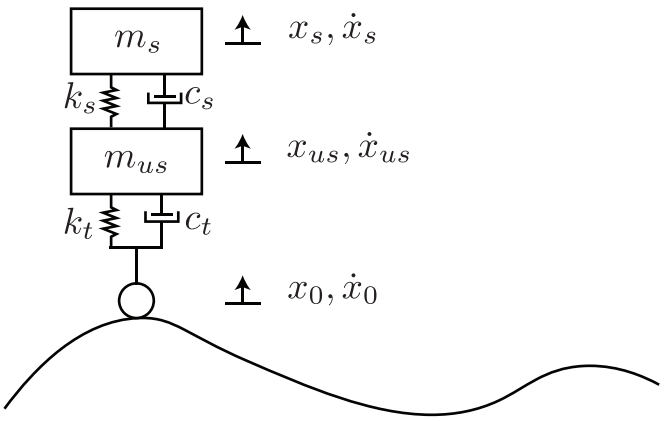

Figure 8: Schematic illustration of the quarter-car model

with the matrix A equal to:

$$A = \begin{bmatrix} 0 & 1 & 0 & 0 \\ \frac{-4k_t}{m_{us}} & \frac{-4(c_s+c_t)}{m_{us}} & \frac{4k_s}{m_{us}} & \frac{4c_s}{m_{us}} \\ 0 & -1 & 0 & 1 \\ 0 & \frac{4c_s}{m_s} & \frac{-4k_s}{m_s} & \frac{-4c_s}{m_s} \end{bmatrix} \tag{36}$$

Four state variables are considered, being respectively the tire deflection $(x_{us} - x_0)$; the unsprung mass velocity $\dot{x}_{us}$; the suspension stroke $x_s - x_{us}$, and sprung mass velocity $\dot{x}_s$. Typically, in the context of assessing the dynamical comfort of a car, two parameters are of interest: the suspension stroke (i.e., the relative displacement of the car body with respect to the unsprung mass) and the acceleration of the sprung mass. In the proceeding study, the damping effect of the tire, c_t is considered negligible. The uncertain road profile $x_0(t)$ is modelled as a precise zero-mean Gaussian random field with squared exponential covariance kernel with a correlation length L of 1 (m) and standard deviation of 1 (mm). Note that a single exponential kernel cannot be used in this case since it is not differentiable at zero-lag.

The dynamics of the car are simulated over a distance of 50 (m), when the car is travelling at a speed of 10 (m/s). The one dimensional spatial domain is discretized into 1000 equidistant points and the time domain is discretized into time intervals of 0.005 (s). In the K-L expansion of $x_0(t)$, a total of 50 dependent Gaussian random variables are used. Considering the limit on the displacement and acceleration of spring mass, the performance function can be established as:

$$
\begin{aligned}
g(\boldsymbol{x},\boldsymbol{y}) &= \min\left\{g_1(\boldsymbol{x},\boldsymbol{y}), g_2(\boldsymbol{x},\boldsymbol{y})\right\} \\
g_1(\boldsymbol{x},\boldsymbol{y}) &= 1 - \max_{i=1,\ldots,m}\left(\frac{x_s(\boldsymbol{x},t_i)-x_{us}(\boldsymbol{x},t_i)}{d}\right) \\
g_2(\boldsymbol{x},\boldsymbol{y}) &= 1 - \max_{i=1,\ldots,m}\left(\frac{\ddot{x}_s(\boldsymbol{x},t_i)}{a}\right)
\end{aligned}
\tag{37}
$$

where $d = 3.5 \times 10^{-3}$(m) and $a = 3.5 \times 10^{-2}(m/s^2)$ are the threshold values for the allowed stroke and acceleration of the sprung mass. The nominal parameters of the state-space model, as well as their uncertainty are listed in table 5. All distributions are truncated such that only non-negative realisations are generated for the physical parameters of the quarter-car model.

Table 5: Parameters of the quarter car state-space model and their uncertainty

Parameter	Mean value	Standard deviation	Distribution
k_s(N/m)	$\theta_1 \in [400, 600]$	50.53	Log-Normal
c_s(N.s/m)	$\theta_2 \in [1600, 2200]$	189.79	Log-Normal
m_s(kg)	325	3.25	Normal
m_{us}(kg)	65	6.5	Normal
k_{us}(N/m)	2325.0	232.5	Log-Normal

4.3.2. Results and discussion

The estimates of the bounds on P_F using ASI-MCS and ASI-SS, as well as the bounds obtained by performing a double loop procedure are shown in Table 6. As noted from the Table, also in this case the bounds on P_F match relatively well, especially taking into account the large gain in computational efficiency obtained with the proposed strategy.

Table 6: Estimated probability bounds and their coefficient of variation for Example 3

Methods	$\hat{P}_F^U$	$Cov(\hat{P}_F^U)$	$\hat{P}_F^L$	$Cov(\hat{P}_F^L)$	N
ASI-MCS	0.0179	0.17	7.3×10^{-3}	0.15	10^4
ASI-SS	0.0158	0.28	7.0×10^{-3}	0.24	2×2000*
Double-loop	0.0160	0.025	7.9×10^{-3}	0.034	$6 \times 10^4 + 59 \times 10^5$

*2×2000 denotes that Subset Simulation required 2 simulation stages, each of them comprising 2000 samples.

As an additional remark, it should be noted that for this particular example, the application of ASI-IS was not explored. While in principle it is possible to apply Importance Sampling to

this problem (see, e.g. [29]), the authors chose not to explore this direction further in order to focus on the assessment of ASI as a general framework and less on the implementation details of a specific Importance Sampling density function.

5. Conclusions

This paper presents a decoupling approach for the propagation of imprecise probabilities based on the concept of the Augmented Space Integral. Rather than aiming at solving the double loop that is typically associated with the propagation of parametric p-boxes, this approach represents the epistemic uncertain parameters by means of an auxilliary distribution to augment the failure probability calculation to the joint space of aleatory and epistemic uncertain parameters. Then, by virtue of Bayes' theorem, an explicit function between the epistemic parameters and the probability of failure of the system can be retrieved. This function is then used to calculate the bounds on the probability of failure.

Following conclusions can be made:

- The proposed approach is numerically more efficient than a typical double loop by several orders of magnitude, however at the cost that the calculated bounds are only approximate.
- The coefficient of variation of the estimator of the probability bounds can be used as a measure for the accuracy of this approximation, allowing for an a posterior accuracy assessment.
- No assumptions on the underlying nature of the structural model were made, making this methodology widely applicable

While the results presented are encouraging, it should be kept in mind that the proposed approach also possesses limitations. Specifically, the number of imprecise distribution parameters that can be handled effectively cannot be that large, e.g. not beyond 10. This is due to the fact that estimating probability densities (as required in the proposed approach) becomes challenging in high dimensions, as documented in [31].

Acknowledgements

Xiukai Yuan would like to acknowledge financial support from NSAF (Grant No. U1530122), the Aeronautical Science Foundation of China (Grant No. ASFC-20170968002). Matthias Faes

gratefully acknowledges the financial support of the Research Foundation Flanders (FWO) under grant number 12P3519N, as well as the Alexander von Humboldt foundation. Marcos Valdebenito acknowledges the support of ANID (National Agency for Research and Development, Chile) under its program FONDECYT, grant number 1180271.

Appendix A. Distribution of $\boldsymbol{\theta}$ conditioned on $(\boldsymbol{x}, \boldsymbol{y})$ and $\boldsymbol{F}$

An expression for $\varphi(\boldsymbol{\theta} \mid \boldsymbol{x}, \boldsymbol{y}, F)$ is next derived. First, using Bayesian theory in the augmented space, it is noted that:

$$\varphi(\boldsymbol{\theta} \mid \boldsymbol{x}, \boldsymbol{y}) = \frac{f(\boldsymbol{x}, \boldsymbol{y} \mid \boldsymbol{\theta})\varphi(\boldsymbol{\theta})}{f(\boldsymbol{x}, \boldsymbol{y})} \tag{A.1}$$

When the probability space is limited to the failure region F instead of the whole augmented space Ω, Eq. (6) becomes:

$$\varphi(\boldsymbol{\theta} \mid (\boldsymbol{x}, \boldsymbol{y}), F) = \frac{f((\boldsymbol{x}, \boldsymbol{y}) \mid \boldsymbol{\theta}, F)\varphi(\boldsymbol{\theta} \mid F)}{f((\boldsymbol{x}, \boldsymbol{y}) \mid F)} \tag{A.2}$$

where $f(\boldsymbol{x}, \boldsymbol{y} \mid \boldsymbol{\theta}, F)$ is the probability density function of $(\boldsymbol{x}, \boldsymbol{y})$ conditional on $\boldsymbol{\theta}$ and F, which is given by:

$$f((\boldsymbol{x}, \boldsymbol{y}) \mid \boldsymbol{\theta}, F) = \frac{I_F(\boldsymbol{x}, \boldsymbol{y}) f((\boldsymbol{x}, \boldsymbol{y}) \mid \boldsymbol{\theta})}{\int I_F(\boldsymbol{x}, \boldsymbol{y}) f((\boldsymbol{x}, \boldsymbol{y}) \mid \boldsymbol{\theta}) d\boldsymbol{x} d\boldsymbol{y}} = \frac{I_F(\boldsymbol{x}, \boldsymbol{y}) f((\boldsymbol{x}, \boldsymbol{y}) \mid \boldsymbol{\theta})}{P_F(\boldsymbol{\theta})} \tag{A.3}$$

And $f((\boldsymbol{x}, \boldsymbol{y}) \mid F)$ is the probability density function of $(\boldsymbol{x}, \boldsymbol{y})$ conditional on F, which is given by:

$$f(\boldsymbol{x}, \boldsymbol{y} \mid F) = \frac{I_F(\boldsymbol{x}, \boldsymbol{y}) f(\boldsymbol{x}, \boldsymbol{y})}{\int I_F(\boldsymbol{x}, \boldsymbol{y}) \int f(\boldsymbol{x}, \boldsymbol{y}, \boldsymbol{\theta}) \mathrm{d}\boldsymbol{\theta} \mathrm{d}\boldsymbol{x} \mathrm{d}\boldsymbol{y}} = \frac{I_F(\boldsymbol{x}, \boldsymbol{y}) f(\boldsymbol{x}, \boldsymbol{y})}{P(F)} \tag{A.4}$$

Substitution of Eqs. (A.3) and (A.4) into Eq. (A.2) leads to the following expression for $\varphi(\boldsymbol{\theta} \mid (\boldsymbol{x}, \boldsymbol{y}), F)$.

$$\varphi(\boldsymbol{\theta} \mid (\boldsymbol{x}, \boldsymbol{y}), F) = I_F(\boldsymbol{x}, \boldsymbol{y}) \frac{f(\boldsymbol{x}, \boldsymbol{y} \mid \boldsymbol{\theta})}{f(\boldsymbol{x}, \boldsymbol{y})} \frac{\varphi(\boldsymbol{\theta} \mid F) P(F)}{P_F(\boldsymbol{\theta})} \tag{A.5}$$

According to Eq. (3), it is noted that $\varphi(\boldsymbol{\theta}) = \varphi(\boldsymbol{\theta}|F)P(F)/P_F(\boldsymbol{\theta})$. Inserting this equality into the last equation, it is found that $\varphi(\boldsymbol{\theta} \mid (\boldsymbol{x}, \boldsymbol{y}), F)$ can be further simplified to:

$$\varphi(\boldsymbol{\theta} \mid (\boldsymbol{x}, \boldsymbol{y}), F) = I_F(\boldsymbol{x}, \boldsymbol{y}) \frac{f(\boldsymbol{x}, \boldsymbol{y} \mid \boldsymbol{\theta})}{f(\boldsymbol{x}, \boldsymbol{y})} \varphi(\boldsymbol{\theta}) \tag{A.6}$$

It is emphasized that the probability density function $\varphi(\boldsymbol{\theta})$ is just a device to yield useful information. It is not meant to reflect the uncertainty associated with $\boldsymbol{\theta}$. Furthermore, it is noted that, without particular preference for the region of the epistemic parameters to be explored, a uniform distribution can be chosen for convenience and leads to appropriate estimates of the FPF [44]. Therefore, it is assumed that $\boldsymbol{\theta}$ is uniformly distributed over its interval support, i.e., $\boldsymbol{\theta} \sim \boldsymbol{U}[\boldsymbol{\theta}^L, \boldsymbol{\theta}^U]$. Thus, $\varphi(\boldsymbol{\theta})$ is a constant within $\boldsymbol{\theta} \in [\boldsymbol{\theta}^L, \boldsymbol{\theta}^U]$. Then, the marginal distribution $f(\boldsymbol{x})$ can be rewritten as:

$$f(\boldsymbol{x}) = \int_{\boldsymbol{\theta}^L}^{\boldsymbol{\theta}^U} f(\boldsymbol{x} \mid \boldsymbol{\theta}) \varphi(\boldsymbol{\theta}) \mathrm{d}\boldsymbol{\theta} = \varphi(\boldsymbol{\theta}) \Delta(\boldsymbol{x}) \tag{A.7}$$

where $\Delta(\boldsymbol{x}) = \int_{\boldsymbol{\theta}^L}^{\boldsymbol{\theta}^U} f(\boldsymbol{x} \mid \boldsymbol{\theta}) \mathrm{d}\boldsymbol{\theta}$ is an integral over the interval support. Note that since all random variables are assumed as independent, calculating this integral is straightforward. For example, it can be calculated using numerical algorithms. An alternative way for expressing $\Delta(\boldsymbol{x})$ is:

$$\Delta(\boldsymbol{x}) = \int_{\boldsymbol{\theta}^L}^{\boldsymbol{\theta}^U} f(\boldsymbol{x} \mid \boldsymbol{\theta}) \mathrm{d}\boldsymbol{\theta} = E_{\boldsymbol{\theta}} \left[\frac{f(\boldsymbol{x} \mid \boldsymbol{\theta})}{\varphi(\boldsymbol{\theta})} \right] \tag{A.8}$$

where $E_{\boldsymbol{\theta}}[\cdot]$ is the expectation under $\varphi(\boldsymbol{\theta})$. This means that $\Delta(\boldsymbol{x})$ can be estimated through sampling. In fact, for the particular case where $\boldsymbol{\theta}$ corresponds to the mean values of Gaussian random variables, $\Delta(\boldsymbol{x})$ can be derived in closed form. Suppose $x_i \sim N\left(\theta_i, \sigma_i^2\right)$, and $\theta_i \sim U\left[\theta_i^L, \theta_i^U\right]$ then $\Delta(\boldsymbol{x})$ is equal to:

$$\Delta(\boldsymbol{x}) = \prod_{i=1}^{n_\theta} \left[\Phi\left(\frac{\theta_i^U - x_i}{\sigma_i} \right) - \Phi\left(\frac{\theta_i^L - x_i}{\sigma_i} \right) \right] \tag{A.9}$$

where $\Phi(\cdot)$ is the cumulative probability function associated with a standard Gaussian distribution.

Substituting Eq. (A.7) into (A.6) and recalling that $\boldsymbol{y}$ is independent from $\boldsymbol{x}$ allows determining the sought posterior distribution $\varphi(\boldsymbol{\theta} \mid (\boldsymbol{x}, \boldsymbol{y}))$, which is equal to:

$$\varphi(\boldsymbol{\theta} \mid \boldsymbol{x}, \boldsymbol{y}) = I_F(\boldsymbol{x}, \boldsymbol{y}) \frac{f(\boldsymbol{x}, \boldsymbol{y} \mid \boldsymbol{\theta}) \varphi(\boldsymbol{\theta})}{f(\boldsymbol{x}, \boldsymbol{y})} = I_F(\boldsymbol{x}, \boldsymbol{y}) \frac{f(\boldsymbol{x} \mid \boldsymbol{\theta}) \varphi(\boldsymbol{\theta})}{f(\boldsymbol{x})} = I_F(\boldsymbol{x}, \boldsymbol{y}) \frac{f(\boldsymbol{x} \mid \boldsymbol{\theta})}{\Delta(\boldsymbol{x})} \tag{A.10}$$

Appendix B. Coefficient of variation of estimator for the failure probability estimator associated with Subset Simulation

This appendix derives the C.o.v. of the estimator $\hat{P}_F(\boldsymbol{\theta})$ in Eq. (23) calculated by the proposed framework with Subset Simulation [41]. For simplicity in notation, let $P_i = P\left(F_i \mid F_{i-1}\right), \hat{P}_i = \hat{P}\left(F_i \mid F_{i-1}\right), i = 1, \ldots, m-1, (\text{ where } F_0 = \Omega), P_m = P(F)$ and $I_{jk}^{(i)} = I_{F_i}\left((\boldsymbol{x}, \boldsymbol{y})_{jk}^{(i-1)}\right)$ where $(\boldsymbol{x}, \boldsymbol{y})_{jk}^{(i-1)}$ denotes the k -th sample in the j -th Markov chain at simulation level $(i-1)$. Thus:

1) Variance of $\hat{P}_1$

As the first stage of Subset Simulation involves Monte Carlo simulation, the variance is simply given as [41]:

$$\mathrm{Var}\left(\hat{P}_1\right) = \frac{P_1(1-P_1)}{N} \approx \frac{\hat{P}_1(1-\hat{P}_1)}{N} \tag{B.1}$$

2) Variance of $\hat{P}_i$ $(2 \leq i \leq m-1)$

At the $(i-1)$-th level, suppose that a number of N_C Markov chains is used and N/N_C samples are generated for each of these chains. Under the assumption that the samples generated by different chains are uncorrelated, the variance of $\hat{P}_i$ $(i = 2, \ldots, m-1)$ is given by [41] :

$$\mathrm{Var}\left(\hat{P}_i\right) = \frac{R_i(0)}{N}\left[1 + 2\sum_{k=1}^{N/N_C-1}\left(1 - \frac{kN_C}{N}\right)\frac{R_i(k)}{R_i(0)}\right] \tag{B.2}$$

Based on the Markov chain samples $\left\{(\boldsymbol{x},\boldsymbol{y},\boldsymbol{\theta})_{jk}^{(i-1)} : j = 1,\ldots,N_c; k = 1,\ldots,N/N_C\right\}$ at the $(i-1)$-th conditional level, the covariance $R_i(k)$ can be estimated as:

$$\hat{R}_i(k) = \left(\frac{1}{N - kN_C}\sum_{j=1}^{N_C}\sum_{l=1}^{N/N_C-k} I_{jl}^{(i)} I_{j,l+k}^{(i)}\right) - \hat{P}_i^2 \tag{B.3}$$

3) Variance of $\hat{P}_m(\boldsymbol{\theta})$

For the last stage of Subset Simulation and for simplicity in notation, let $V_{jk}^{(i)} = \frac{I_F\left(\boldsymbol{x}^{(j)},\boldsymbol{y}^{(j)}\right) f\left(\boldsymbol{x}^{(j)}|\boldsymbol{\theta}\right)}{\Delta\left(\boldsymbol{x}^{(j)}\right)}$ and $\hat{P}_m = \hat{P}_m(\boldsymbol{\theta})$. Then the variance of $\hat{P}_m$ is given by [41]:

$$\mathrm{Var}\left(\hat{P}_m\right) = \frac{R_m(0)}{N}\left[1 + 2\sum_{k=1}^{N/N_C-1}\left(1 - \frac{kN_C}{N}\right)\frac{R_m(k)}{R_m(0)}\right] \tag{B.4}$$

Based on the Markov chain samples $\left\{(\boldsymbol{x},\boldsymbol{\theta})_{jk}^{(m-1)} : j = 1,\ldots,N_C; k = 1,\ldots,N/N_C\right\}$ at the $(m-1)$-th conditional level, the covariance $R_m(k)$ is estimated as:

$$R_m(k) \approx \hat{R}_m(k) = \left(\frac{1}{N - kN_C}\sum_{j=1}^{N_C}\sum_{l=1}^{N/N_C-k} V_{jl}^{(m)} V_{j,l+k}^{(m)}\right) - \hat{P}_m^2 \tag{B.5}$$

4) C.o.v. of $\hat{P}_F(\boldsymbol{\theta})$

At last, suppose all $\hat{P}_i$ $(i = 1,\ldots,m)$ are uncorrelated [41], then the C.o.v. of $\hat{P}_F(\boldsymbol{\theta})$ is given by:

$$\mathrm{Cov}\left[\hat{P}_F(\boldsymbol{\theta})\right] = \sqrt{\sum_{i=1}^{m}\frac{\mathrm{Var}\left(\hat{P}_i\right)}{P_i^2}} \approx \sqrt{\sum_{i=1}^{m}\frac{\mathrm{Var}\left(\hat{P}_i\right)}{\hat{P}_i^2}} \tag{B.6}$$

where $\mathrm{Var}\left(\hat{P}_i\right)$ can be calculated according to Eqs. (B.1),(B.2) and (B.4).

References

[1] M. Beer, S. Ferson, V. Kreinovich, Imprecise probabilities in engineering analyses, Mechanical Systems and Signal Processing 37 (2013) 4–29.

[2] S. Ferson, V. Kreinovich, L. Ginzburg, D. S. Myers, K. Sentz, Constructing Probability Boxes and Dempster-Shafer Structures, Technical Report January, Technical report, Sandia National Laboratories, 2003.

[3] Y. C. Yin, F. P. Coolen, T. Coolen-Maturi, An imprecise statistical method for accelerated life testing using the power-Weibull model, Reliability Engineering and System Safety 167 (2017) 158–167. doi:10.1016/j.ress.2017.05.045.

[4] C. Simon, F. Bicking, Hybrid computation of uncertainty in reliability analysis with p-box and evidential networks, Reliability Engineering and System Safety 167 (2017) 629–638. doi:10.1016/j.ress.2017.04.015.

[5] J. Mullins, Y. Ling, S. Mahadevan, L. Sun, A. Strachan, Separation of aleatory and epistemic uncertainty in probabilistic model validation, Reliability Engineering and System Safety 147 (2016) 49–59. doi:10.1016/j.ress.2015.10.003.

[6] M. Broggi, M. Faes, E. Patelli, Y. Govers, D. Moens, M. Beer, Comparison of Bayesian and interval uncertainty quantification: Application to the AIRMOD test structure, in: 2017 IEEE Symposium Series on Computational Intelligence, SSCI 2017 - Proceedings, volume 2018-Janua, 2018, pp. 1–8. doi:10.1109/SSCI.2017.8280882.

[7] A. Mancuso, M. Compare, A. Salo, E. Zio, T. Laakso, Risk-based optimization of pipe inspections in large underground networks with imprecise information, Reliability Engineering and System Safety 152 (2016) 228–238. doi:10.1016/j.ress.2016.03.011.

[8] M. Faes, D. Moens, Imprecise random field analysis with parametrized kernel functions, Mechanical Systems and Signal Processing 134 (2019) 106334. doi:10.1016/j.ymssp.2019.106334.

[9] W. Gao, D. Wu, C. Song, F. Tin-Loi, X. Li, Hybrid probabilistic interval analysis of bar structures with uncertainty using a mixed perturbation Monte-Carlo method, Finite Elements in Analysis and Design 47 (2011) 643–652.

[10] B. Xia, D. Yu, J. Liu, Hybrid uncertain analysis for structural-acoustic problem with random and interval parameters, Journal of Sound and Vibration 332 (2013) 2701–2720. doi:10.1016/j.jsv.2012.12.028.

[11] S. Yin, D. Yu, Z. Luo, B. Xia, Unified polynomial expansion for interval and random response analysis of uncertain structure-acoustic system with arbitrary probability distribution, Computer Methods in Applied Mechanics and Engineering 336 (2018) 260–285.

[12] J. Wu, Y. Zhang, L. Chen, Z. Luo, A Chebyshev interval method for nonlinear dynamic systems under uncertainty, Applied Mathematical Modelling 37 (2013) 4578–4591.

[13] M. C. M. Troffaes, Imprecise Monte Carlo simulation and iterative importance sampling for the estimation of lower previsions, International Journal of Approximate Reasoning 101 (2018) 31–48. doi:https://doi.org/10.1016/j.ijar.2018.06.009.

[14] A. Decadt, G. de Cooman, J. De Bock, Monte Carlo Estimation for Imprecise Probabilities: Basic Properties (2019). URL: http://arxiv.org/abs/1905.09301. arXiv:1905.09301.

[15] Y. T. Zhou, C. Jiang, X. Han, Interval and subinterval analysis methods of the structural analysis and their error estimations, International Journal of Computational Methods 3 (2006) 229–244.

[16] R. Schöbi, B. Sudret, Structural reliability analysis for p-boxes using multi-level meta-models, Probabilistic Engineering Mechanics 48 (2017) 27–38.

[17] R. Schöbi, B. Sudret, Global sensitivity analysis in the context of imprecise probabilities (p-boxes) using sparse polynomial chaos expansions, Reliability Engineering & System Safety 187 (2019) 129–141. doi:https://doi.org/10.1016/j.ress.2018.11.021.

[18] L. V. Utkin, F. P. Coolen, A robust weighted SVR-based software reliability growth model, Reliability Engineering and System Safety 176 (2018) 93–101.

[19] M. Faes, J. Sadeghi, M. Broggi, M. de Angelis, E. Patelli, M. Beer, D. Moens, On the Robust Estimation of Small Failure Probabilities for Strong Nonlinear Models, ASCE-ASME J Risk and Uncert in Engrg Sys Part B Mech Engrg 5 (2019). doi:10.1115/1.4044044.

[20] J. Sadeghi, M. de Angelis, E. Patelli, Robust propagation of probability boxes by interval predictor models, Structural Safety 82 (2020) 101889.

[21] P. Wei, J. Song, S. Bi, M. Broggi, M. Beer, Z. Lu, Z. Yue, Non-intrusive stochastic analysis with parameterized imprecise probability models: I. Performance estimation, Mechanical Systems and Signal Processing 124 (2019) 349–368.

[22] P. Wei, J. Song, S. Bi, M. Broggi, M. Beer, Z. Lu, Z. Yue, Non-intrusive stochastic analysis with parameterized imprecise probability models: II. Reliability and rare events analysis, Mechanical Systems and Signal Processing 126 (2019) 227–247.

[23] M. G. R. Faes, M. A. Valdebenito, Fully decoupled reliability-based design optimization of structural systems subject to uncertain loads, Computer Methods in Applied Mechanics and Engineering 371 (2020) 113313.

[24] M. G. R. Faes, M. A. Valdebenito, D. Moens, M. Beer, Operator norm theory as an efficient tool to propagate hybrid uncertainties and calculate imprecise probabilities, Mechanical Systems and Signal Processing (2020, accepted).

[25] M. G. Faes, M. A. Valdebenito, D. Moens, M. Beer, Bounding the first excursion probability of linear structures subjected to imprecise stochastic loading, Computers & Structures 239 (2020) 106320. doi:10.1016/j.compstruc.2020.106320.

[26] S. K. Au, Probabilistic failure analysis by importance sampling Markov chain simulation, Journal Of Engineering Mechanics 130 (2004) 303–311.

[27] J. Ching, Y.-H. Hsieh, Local estimation of failure probability function and its confidence interval with maximum entropy principle, Probabilistic Engineering Mechanics 22 (2007) 39–49.

[28] J. Ching, Y.-H. Hsieh, Approximate reliability-based optimization using a three-step approach based on subset simulation, Journal of engineering mechanics 133 (2007) 481–493.

[29] H. A. Jensen, M. A. Valdebenito, G. I. Schuëller, An Efficient Reliability-Based Optimization Scheme for Uncertain Linear Systems subject to General Gaussian Excitation, Computer Methods in Applied Mechanics and Engineering 198 (2008) 72–87.

[30] A. A. Taflanidis, J. L. Beck, Analytical approximation for stationary reliability of certain and uncertain linear dynamic systems with higher-dimensional output, Earthquake Engineering & Structural Dynamics 35 (2006) 1247–1267. doi:10.1002/eqe.581.

[31] P. S. Koutsourelakis, Design of complex systems in the presence of large uncertainties: A statistical approach, Computer Methods in Applied Mechanics and Engineering 197 (2008) 4092–4103.

[32] X. Yuan, S. Liu, M. A. Valdebenito, J. Gu, M. Beer, Efficient framework for failure probability function estimation in augmented space, preprint submitted to Elsevier (2020).

[33] J. Song, P. Wei, M. Valdebenito, S. Bi, M. Broggi, M. Beer, Z. Lei, Generalization of non-intrusive imprecise stochastic simulation for mixed uncertain variables, Mechanical Systems and Signal Processing 134 (2019) 106316. doi:https://doi.org/10.1016/j.ymssp.2019.106316.

[34] J. Zhang, M. D. Shields, On the quantification and efficient propagation of imprecise probabilities with copula dependence (2019). URL: http://arxiv.org/abs/1805.12525. arXiv:1805.12525.

[35] M. G. R. Faes, M. A. Valdebenito, X. Yuan, P. Wei, M. Beer, Augmented Reliability Analysis for Estimating Imprecise First Excursion Probabilities in Stochastic Linear Dynamics, preprint submitted to elsevier (2020).

[36] M. A. Misraji, M. A. Valdebenito, H. A. Jensen, C. F. Mayorga, Application of directional importance sampling for estimation of first excursion probabilities of linear structural systems subject to stochastic Gaussian loading, Mechanical Systems and Signal Processing 139 (2020) 106621. doi:10.1016/j.ymssp.2020.106621.

[37] R. Lebrun, A. Dutfoy, Do Rosenblatt and Nataf isoprobabilistic transformations really differ?, Probabilistic Engineering Mechanics 24 (2009) 577–584. doi:10.1016/j.probengmech.2009.04.006.

[38] G. I. Schuëller, H. J. Pradlwarter, Benchmark Study on Reliability Estimation in Higher Dimensions of Structural Systems – An Overview, Structural Safety 29 (2007) 167–182.

[39] K. Marti, Approximation and derivatives of probabilities of survival in structural analysis and design, Structural Optimization 13 (1997) 230–243.

[40] K. Breitung, Asympotic Approximations for Probability Integrals, Probabilistic Engineering Mechanics 4 (1989) 187–190.

[41] S. K. Au, J. L. Beck, Estimation of Small Failure Probabilities in High Dimensions by Subset Simulation, Probabilistic Engineering Mechanics 16 (2001) 263–277.

[42] X. Yuan, Z. Lu, C. Zhou, Z. Yue, A novel adaptive importance sampling algorithm based on Markov chain and low-discrepancy sequence, Aerospace Science and Technology 29 (2013) 253–261. doi:https://doi.org/10.1016/j.ast.2013.03.008.

[43] J. Li, J.-B. Chen, The probability density evolution method for dynamic response analysis of non-linear stochastic structures, International Journal for Numerical Methods in Engineering 65 (2006) 882–903. doi:10.1002/nme.1479.

[44] S. Au, Reliability-based design sensitivity by efficient simulation, Computers & structures 83 (2005) 1048–1061.

[45] S.-K. Au, J. L. Beck, A new adaptive importance sampling scheme for reliability calculations, Structural safety 21 (1999) 135–158.

[46] S.-K. Au, J. L. Beck, Estimation of small failure probabilities in high dimensions by subset simulation, Probabilistic engineering mechanics 16 (2001) 263–277.

[47] S. Xiao, Z. Lu, Structural reliability analysis using combined space partition technique and unscented transformation, Journal of Structural Engineering 142 (2016) 04016089.

[48] X. Yuan, Local estimation of failure probability function by weighted approach, Probabilistic Engineering Mechanics 34 (2013) 1–11.